ACS APPLIED MATERIALS & INTERFACES

Research Article

www.acsami.org

Aqueous Dispersible Graphene/Pt Nanohybrids by Green Chemistry: Application as Cathodes for Dye-Sensitized Solar Cells

Young-Gon Kim,[†,‡] Zico Alaia Akbar,[§] Dong Young Kim,[†,‡] Seong Mu Jo,[†,‡] and Sung-Yeon Jang*[,§]

[†]Center for Materials Architecturing, Korea Institute of Science and Technology, 39-1 Hawolgok-dong, Seong-buk, Seoul, Korea
[‡]Nanomaterials Science and Engineering, University of Science and Technology, 176 Gajeong-dong, Yuseong-gu, Daejeon, Korea
[§]Department of Chemistry, Kookmin University, 861-1 Jeongneung-dong, Seong-buk, Seoul, Korea

Supporting Information

ABSTRACT: Aqueous dispersible nanohybrids (NHBs) of graphene nanosheets (GNSs) and Pt nanoparticles (Pt-NPs) were synthesized through the one-pot reduction of their precursors using an environmentally benign chemical, vitamin C. The concurrent reduction of the precursors, which includes graphene oxide (GO) to GNS and H_2PtCl_6 to Pt^0, was facile and efficient to yield GNS/Pt-NHBs in which face-centered cubic (fcc) crystalline Pt-NPs with average diameters of ~5 nm were robustly attached on the surface of the GNSs. The conversion yield during Pt reduction was fairly high (~90%) and the Pt content within the NHBs was easily controllable. The resulting stable aqueous colloidal dispersion of GNS/Pt-NHBs was successfully fabricated as thin films without using any binder by the electro-spray method at room temperature, and the fabricated samples were used as counter electrodes (CEs) for dye-sensitized solar cells (DSSCs). The electrocatalytic activity of the NHBs for I^-/I_3^- redox couples in conventional DSSCs was investigated using cyclic voltammetry (CV) and electrochemical impedance spectroscopy (EIS) analysis. Doping of GNSs with small amounts of Pt-NPs (<10 wt %) could dramatically enhance the redox kinetics. The enhanced electrocatalytic activity of the GNS/Pt-NHBs was reflected in the performance of the DSSCs. The power conversion efficiency of optimized DSSCs using the NHB-CEs was 8.91% (V_{OC}: 830 mV, J_{SC}: 15.56 mAcm^{-2}, and FF: 69%), which is comparable to that of devices using the state-of-the-art Pt-based CEs (8.85%).

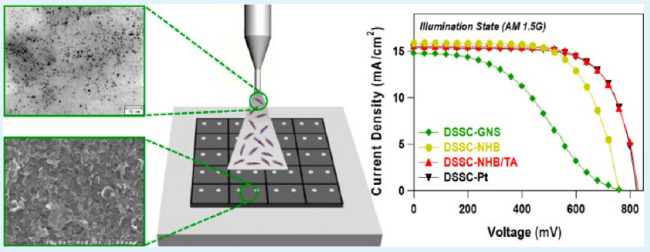

KEYWORDS: *graphene nanosheet, platinum, dye-sensitized solar cell, counter electrode, electrocatalytic activity*

INTRODUCTION

Dye-sensitized solar cells (DSSCs) are one among the attractive next-generation solar cells owing to its simple low-cost fabrication and high energy conversion efficiency.[1,2] In typical DSSCs, the electrons are injected from photo-oxidized dyes into photoelectrodes (typically TiO_2 nanoparticles), and the resulting oxidized dyes are regenerated by electrolytes. In a typical electrolyte, I^- ions reduce the oxidized dyes, yielding I_3^-, and the resulting I_3^- ions are finally reduced to I^- at a counter electrode (CE).[2−4] Thus, the efficient reduction of I_3^- at CEs is an important requisite to achieve high-efficiency DSSCs. With respect to research on other major components of DSSCs such as dyes, photoelectrodes, and electrolytes, the researches on CEs have been relatively few. Pt has been a cornerstone material for CEs owing to its high catalytic activity, although its high cost is an ongoing cause for concern.[5] Pt-based CEs (Pt-CEs) have typically been prepared either by thermal annealing of a Pt precursor solution (at higher than 400 °C) or sputtering onto fluorine-doped tin oxide (FTO) coated glass, which requires either a high temperature or a vacuum environment, thus increasing the final cost.[6,7]

Because simple, low-cost, room-temperature fabrication processes are of pivotal interest for DSSC commercialization, much effort is being made to either replace Pt with less expensive alternative materials or develop easier low-temperature methods with reduced Pt loading. A range of carbonaceous materials, including carbon nanotubes (CNTs) and graphene,[8−15] and electrically conductive polymers such as poly(3,4-alkylenedioxythiophene),[16−18] polyaniline,[19,20] and polypyrrole[21] have been tested for use as CEs. Recently, hybrids of conductive polymers and nanocarbon materials were also successfully applied, capitalizing on their respective advantages.[22−24] These materials displayed reasonable CE performance in electrolytes containing I^-/I_3^- redox couples. In the case of nanocarbons, their high surface area could compensate for the sluggish electrocatalytic reaction rate compared to that of Pt. Improving the degree of exfoliation and solution processability are crucial requirements in order to capitalize on the potential of nanocarbon materials.[11] The performance of conductive polymer based CEs for the I^-/I_3^- redox couple has not been as good as that of Pt-CEs; however,

Received: December 2, 2012
Accepted: February 8, 2013
Published: February 8, 2013

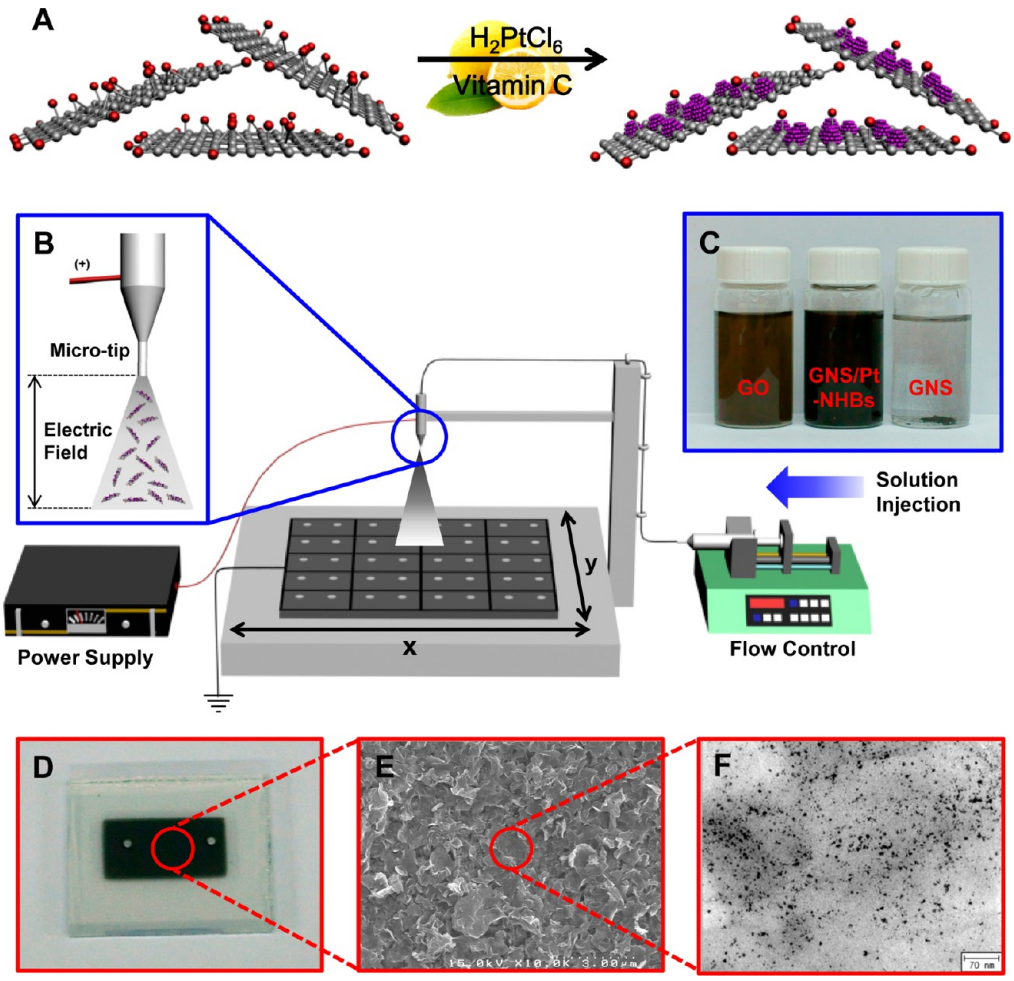

Figure 1. Schematic description of the preparation of GNS/Pt-NHB-based CEs. (A) Synthetic strategy for the GNS/Pt-NHB preparation; (B) e-spray method for NHB deposition; (C) Photos of GO, GNS, and GNS/Pt-NHBs in aqueous media (concentration of all solution was 0.3 mg mL^{-1}); (D) photo of the resulting GNS/Pt-NHB-based CEs by e-spray; (E) SEM image of the NHBs; (F) TEM image of the NHBs.

their potential for chemical structure modification promises further improvement.[17,22]

Recently, Pt-dispersed hybrid materials have been actively investigated in order to achieve cost-effective CEs with reduced Pt loading.[25,26] Hybridization of Pt with polymers, metal oxides, and nanocarbons has been reported, and it is found to provide promising results.[21,27−33] Among them, graphene has been a very attractive material because this thin 2D structure has a high specific surface area and sufficient electrical conductivity.[34,35] The unique properties of graphene have been implemented in transparent conducting electrodes,[36,37] transistors,[38] sensors,[39,40] and electrochemical devices.[41−43] Hybridization of graphene with Pt nanoparticles (Pt-NPs) has been an emerging strategy to obtain synergistic effects of the two components while overcoming the intrinsic limitations of the individual materials. Graphene serves as an excellent support for Pt-NPs owing to its high surface area, which helps to manifest the catalytic function of Pt-NPs. The resulting synergy has been successfully demonstrated in a range of applications that require the high catalytic activity of Pt-NPs such as fuel cells,[44−46] electrochemical biosensors,[47,48] and catalysts for chemical reactions.[49,50]

A few studies on the use of graphene/Pt hybrids as CEs for DSSCs (DSSC−CEs) have recently been reported.[31−33] In these reports, different strategies were attempted to obtain the hybrids. For example, multistep deposition provided a straightforward route for hybridization. Bajpai et al. prepared the hybrids by depositing Pt-NPs using pulsed laser deposition (PLD) onto chemically prepared graphene layers,[33] whereas Gong et al. used a layer-by-layer assembly technique, followed by thermal reduction to prepare the graphene/polyelectrolyte/Pt hybrids.[31]

The resulting hybrid-based CEs displayed enhanced performance when compared to that exhibited by graphene-only CEs prepared by an identical deposition method. One-pot preparation of graphene/metal-NP hybrids under appropriate chemical/thermal conditions is a recently emerging strategy.[44,45,47,48] Yen *et al.* simultaneously reduced graphene oxide (GO) and a Pt precursor using a chemical reduction agent under a high temperature (120 °C) and used the resulting specimens as CEs.[32] Development of easy and environmentally benign methods to prepare graphene/Pt hybrids with controllable Pt loading and dispersion will widely contribute to various applications, including DSSCs.

In this study, aqueous dispersible nanohybrids (NHBs) of graphene nanosheets (GNSs) and Pt (i.e., GNS/Pt-NHBs) were synthesized by a one-pot reaction. Concurrent co-reduction of GO and a Pt precursor (H_2PtCl_6) was successfully achieved in water using vitamin C, an environmentally friendly chemical. The resulting NHBs retained the individual character-

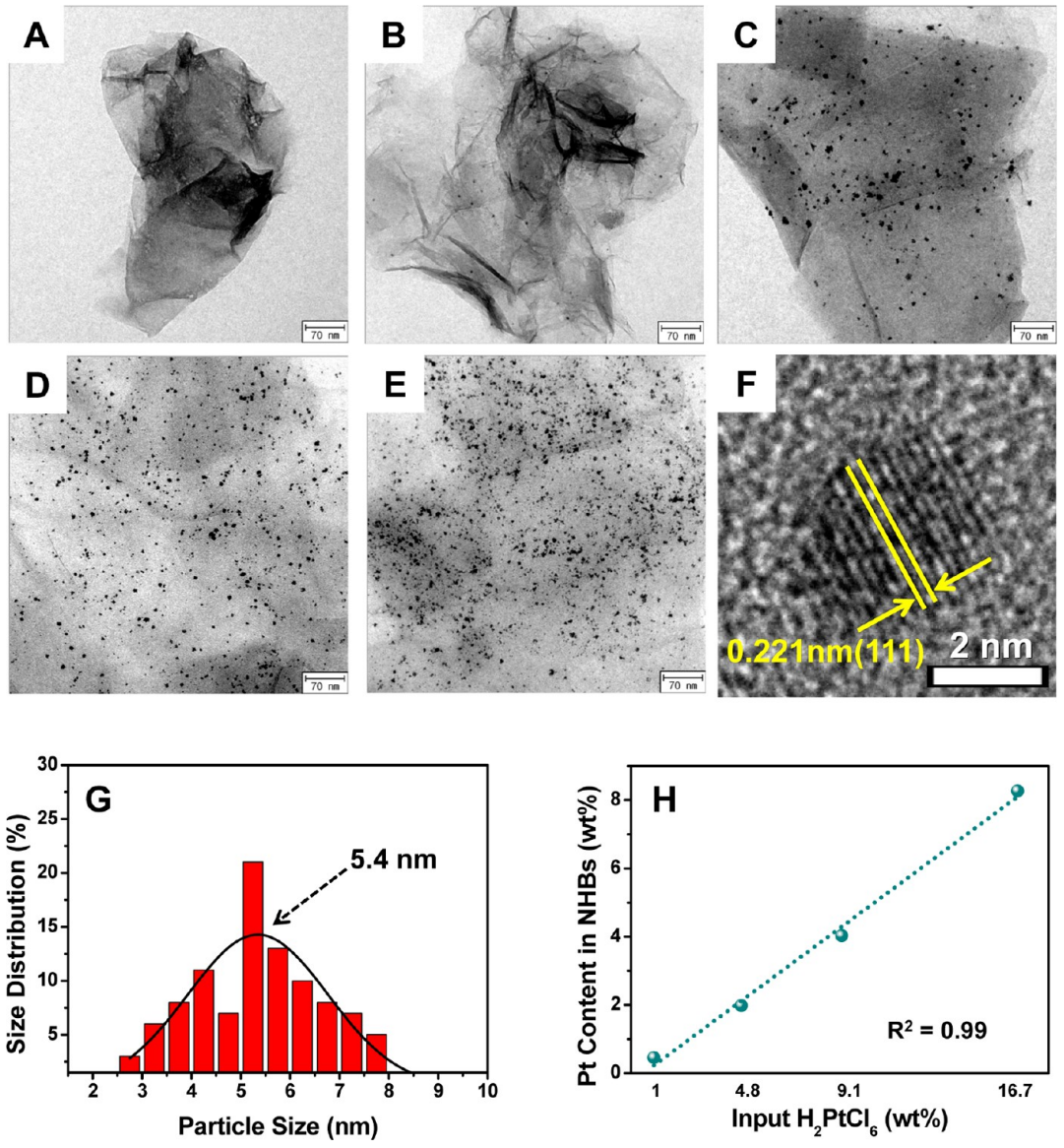

Figure 2. TEM images of (A) GNS and (B–E) GNS/Pt-NHBs. The Pt loading levels of the TEM images of NHBs are (B) 1 wt % (GNS/Pt1), (C) 5 wt % (GNS/Pt5), (D) 10 wt % (GNS/Pt10), and (E) 20 wt % (GNS/Pt20). (F) High-resolution TEM image of GNS/Pt-NHBs. (G) Particle size distribution of GNS/Pt-NHBs (GNS/Pt20). (H) The relationship between input amount (wt %) of Pt precursor for the synthesis and the resulting loading level (wt %) of Pt-NPs on the GNS/Pt-NHBs.

istics of both compounds as well as enhanced solubility (dispersibility) in water. The formation of GNS/Pt-NHBs was confirmed by X-ray diffraction (XRD) analysis, Fourier transform infrared spectroscopy (FT-IR), Raman spectroscopy, and X-ray photoelectron spectroscopy (XPS). The morphology of the NHBs, in which Pt-NPs with diameters of several nanometers were evenly distributed on the surface of the GNSs, was revealed by transmission electron microscopy (TEM) and scanning electron microscopy (SEM) images. The amount of Pt-NPs in the NHBs was linearly proportional to that of the loaded precursors, as confirmed by inductively coupled plasma atomic emission spectroscopy (ICP-AES). The thin-film CEs of GNS/Pt-NHBs were fabricated by the electrostatic spray (e-spray) method directly from the stable aqueous colloidal NHB solutions at room temperature (RT) without using any binder. The enhanced electrocatalytic activity for I^-/I_3^- redox couples of DSSCs by the hybridization of Pt-NPs with GNSs was indicated by cyclic voltammetry (CV) and electrochemical impedance spectroscopy (EIS) analysis. The DSSCs using the optimized GNS/Pt-NHB thin films as CEs exhibited a power conversion efficiency (PCE) of 8.91% with an open circuit voltage (V_{OC}), short circuit photocurrent density (J_{SC}), and fill factor (FF) of 830 mV, 15.56 mA cm^{-2}, and 69%, respectively. This result is comparable to the performance of DSSCs using state-of-the-art Pt-CEs (PCE 8.85%).

RESULTS AND DISCUSSION

Preparation of GNS/Pt-NHBs. A schematic description of our study is depicted in Figure 1. NHBs of GNS and Pt-NPs were prepared by a one-pot reaction in aqueous media at RT through chemical reduction of their precursors using vitamin C. The aqueous dispersion of GO was prepared by the oxidation of graphite via Hummer's method,[51,52] followed by ultrasonication. To prepare the GNS/Pt-NHBs, we mixed aqueous solutions of H_2PtCl_6 (a precursor for Pt) with the GO solutions, and then vitamin C was added into the mixture for

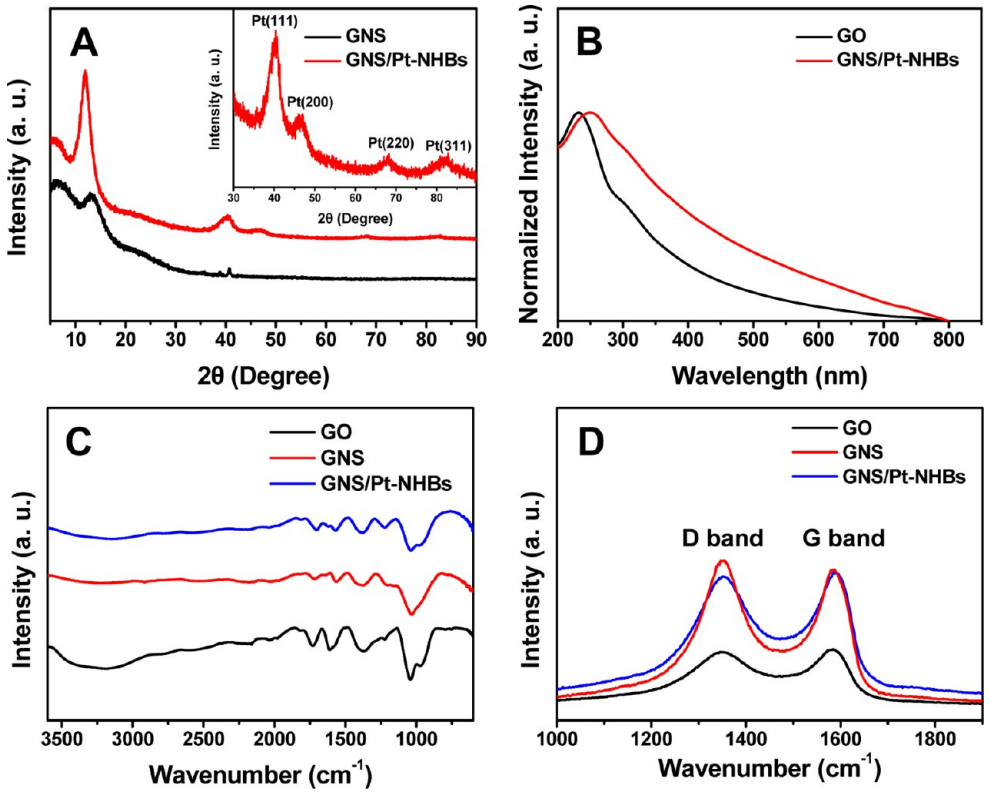

Figure 3. (A) XRD analysis results of GNS and GNS/Pt-NHBs (GNS/Pt20). Spectroscopic analysis results of GNS/Pt-NHBs: (B) UV−vis spectra of GO and GNS/Pt-NHBs; (C) FT-IR spectra and (D) Raman spectra of GO, GNS, and GNS/Pt-NHBs.

simultaneous reduction of both precursors. After stirring the mixture for 48 h at RT, the color of the solution turned from yellowish brown to black, which indicated the reduction of GO to GNS (Figure 1C). The resulting solution was maintained as a stable colloid over a relatively wide range of concentrations (0.1−0.5 mg mL^{-1}), as confirmed by the zeta potential values at pH 7 (less than −33 mV). As shown in Figure 1C, the control aqueous GNS solution prepared by an identical procedure without Pt precursors exhibited reduced colloidal stability with aggregation. The enhancement of the colloidal stability of GNS/Pt-NP hybrids (or other metal particles) through the facilitated exfoliation by NPs among graphene sheets have been reported in earlier studies.[44,53] However, this is the first report of the simultaneous reduction of GO and a Pt precursor to prepare NHBs by a one-pot reaction at RT using vitamin C.

Analysis of GNS/Pt-NHBs. Figure 2 shows the bright-field TEM images of GNS/Pt-NHBs over a range of GNS/Pt ratios. The relatively uniform and fine Pt-NPs with diameters of several nanometers were well dispersed on the surface of the GNSs that were mainly composed of one to a few layers of graphene. The mean diameter of the Pt particles was ∼5.4 nm, and the distribution of the diameter is shown in Figure 2G. The d-spacing of the lattice fringe was 0.221 nm, which corresponds to the d_{111} interplanar distance of face-centered cubic (fcc) crystalline Pt, as shown in the inserted high-resolution image in Figure 2F. The XRD patterns of the NHBs in Figure 3A confirmed the presence of crystalline Pt on the GNSs. The prominent peaks corresponding to the (111), (200), (220), and (311) diffraction peaks of fcc Pt (JCPDS:87-0647) indicated that the Pt exists in the form of crystalline state (refer the inset of Figure 3A), while a (002) peak ($2\theta \approx 20-30°$) confirmed the formation of the GNSs (Figure 3A). Notably, the (002) peak of the GNS/Pt-NHBs was broader than that of the GNSs, which indicates the higher exfoliation/solvation degree of GNSs in NHBs than in GNSs alone due to the foreign moieties.[53] This result also corresponds to the enhanced colloidal stability of the NHBs in aqueous solutions compared to GNSs (Figure 1C). The high robustness of the NHBs was notable. The density of Pt-NPs on the GNS surface was maintained after long-term ultrasonication (>1 h) of the NHB solutions followed by centrifugation. The strong adsorption energy of Pt-NPs on the defect sites of carbon nanomaterials has previously been reported.[54] The size and distribution of the Pt-NPs were relatively independent of the amount of vitamin C used, the GO/H_2PtCl_6 ratio in the reaction mixture, and the reaction time for reduction, which indicates that the formation of Pt-NPs in NHBs was rapid and straightforward. The amount of Pt-NPs attached on the GNSs with respect to the input ratio of the two precursors was characterized using ICP-AES. The resulting Pt content of the NHBs was linearly proportional to the amount of the Pt precursor used for the reduction (Figure 2H). The conversion yield of input H_2PtCl_6 to output Pt was found to be ∼90 % in all samples in this study. This fact implies that the reduction to Pt by vitamin C is facile and the amount of Pt in NHBs can be easily controllable.

The successful reduction of GO to GNSs during the NHB formation was investigated. The redshift of the maximum absorption peaks in the UV-vis spectra from approximately 230 nm to 260 nm (Figure 3B) indicated the significant restoration of π-conjugation[55] in the NHBs through the reduction of GO. The FT-IR spectra in Figure 3C indicate a significant reduction in oxygen functionality in the NHBs, such as a C═O stretching vibration peak at 1732 cm^{-1}, the vibration and deformation peaks of O−H groups at 3395 and 1381 cm^{-1}, and the C−O

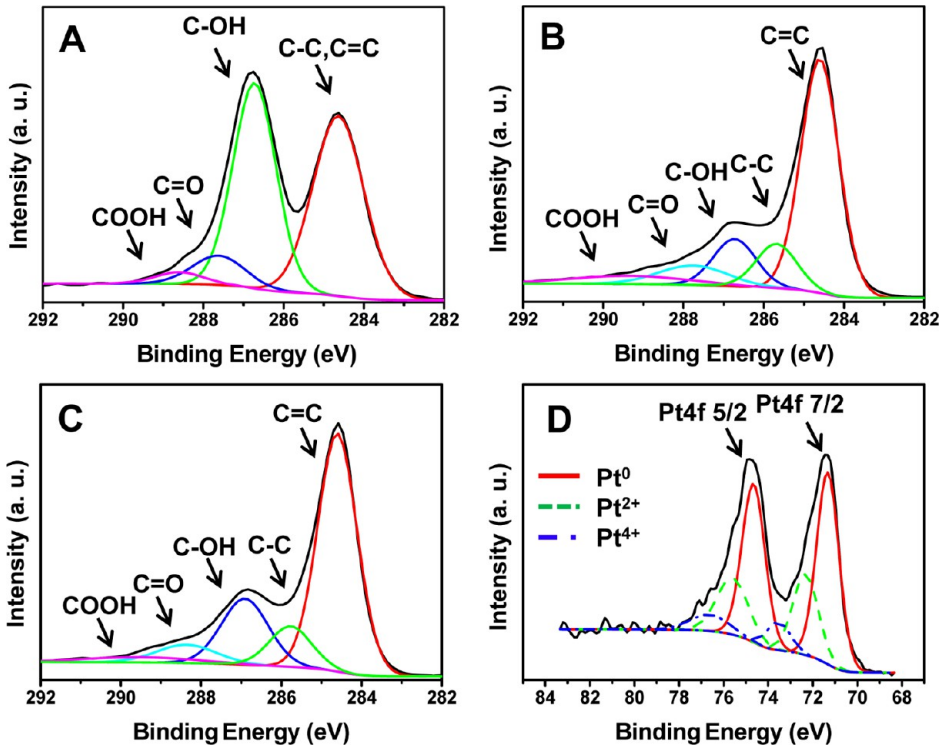

Figure 4. XPS Spectra (C1s) of (A) GO, (B) GNS, (C) GNS/Pt-NHBs (GNS/Pt20), and (D) Pt4f Spectrum of GNS/Pt-NHBs (GNS/Pt20).

stretching peak at 1223 and 1039 cm^{-1}. The similarity of the FT-IR spectra of the NHBs and GNSs revealed that the reduction of GO in the NHBs was as efficient as that in the GNSs. The change of the surface functional groups of GO upon reduction was further investigated using XPS (Figure 4). The C1s XPS spectrum of the GNSs clearly indicated the considerable reduction of GO during the formation of the NHBs, including the marginal remaining oxidation.[52,55] The peak corresponding to sp^2 C−C (~284.6 eV) was majorly observed, which implies significant recovery of the basal plane of the GNSs with residual C−O (~286.7 eV), C═O (~287.7 eV), and C═O−O (~289.3 eV).[52,56] The XPS spectra of the NHBs were almost identical to that of the GNSs without Pt, which is in good agreement with the reported results using similar chemistry.[57−59] The C/O ratio of the GO, GNSs, and NHBs determined by the XPS analysis were 2.04, 4.01, and 3.46, respectively. These results confirmed the efficient reduction of oxygen-containing functional groups of GO during NHB formation using vitamin C. Structural changes of GO during the reduction were also characterized by Raman spectroscopy based on the two characteristic absorption bands: the G band at ~1589 cm^{-1} and the D band at ~1352 cm^{-1} (Figure 3D). The G band is associated with bond-stretching of the sp^2 carbon pairs in both rings and chains, whereas the D band is due to the breathing mode of aromatic rings with dangling bonds in plane terminations.[52] The D/G intensity ratio of the NHBs was approximately 0.97−1.08, values that are much higher than that of GO (0.95), suggesting that more sp^2 domains are formed during the reduction to NHBs, which agrees well with previously reported results.[52,58]

Fabrication of NHB-CEs Using e-Spray Method. The high colloidal stability of the GNS/Pt-NHBs in a range of solvents including water and alcohols offers high solution processability for thin-film fabrication. High-quality films of carbon nanomaterials with reduced aggregation were readily achievable when well-dispersed stable solutions were used. Thin films of the NHBs were prepared on a FTO-coated glass plate using the e-spray method (Figure 1B). In our earlier studies, the e-spray method has provided an efficient route to fabricate thin films of carbon nanomaterials such as CNTs and graphene.[11,60] The resulting films had good surface morphology with low thickness variation and their thickness was easily controllable. Furthermore, this method is a RT process and requires no binder, with reduced material consumption.[11,61] Our aqueous NHB solutions were stable enough to use the e-spray method for film deposition. The deposition could be continuously performed for more than 24 h without clogging the nozzle, and the resulting film thickness was proportional to the deposition time. Figure 1D shows the NHB thin films e-sprayed on the FTO/glass using a 0.16 mg mL^{-1} NHB solution in a DI-water/ethanol (6/4) solution. The samples showed good uniformity, possessing an open and layered morphology without macro-aggregation, as shown in the SEM images (Figure 1E). The specific surface area and pore volume of the films, which were analyzed using the Brunauer−Emmett−Teller (BET) and Barrett−Joyner−Halenda (BJH) methods, were 158 $m^2\ g^{-1}$ and 0.617 $cm^3\ g^{-1}$, respectively.

Electrocatalytic Activity of NHB-CEs toward the I^-/I_3^- Redox Reactions. In DSSCs, the I^-/I_3^- couple has been widely used as the redox medium for continuous regeneration of sensitizers. The sufficient electrocatalytic activity toward the reduction of I_3^- ions to I^- ions is a crucial factor for efficient CEs. The electrocatalytic performance of the NHB thin films on the reduction of I_3^- ions was characterized using electrochemical impendence spectroscopy (EIS). Figure 5 shows the Nyquist plots by the EIS analysis of symmetric cells and the equivalent circuit diagram used for the simulation. For the symmetric cells, the e-sprayed NHB and GNS thin film-based CEs (NHB-CE and GNS-CE) were used as the working electrodes, in which the electrolyte solution containing I^-/I_3^-

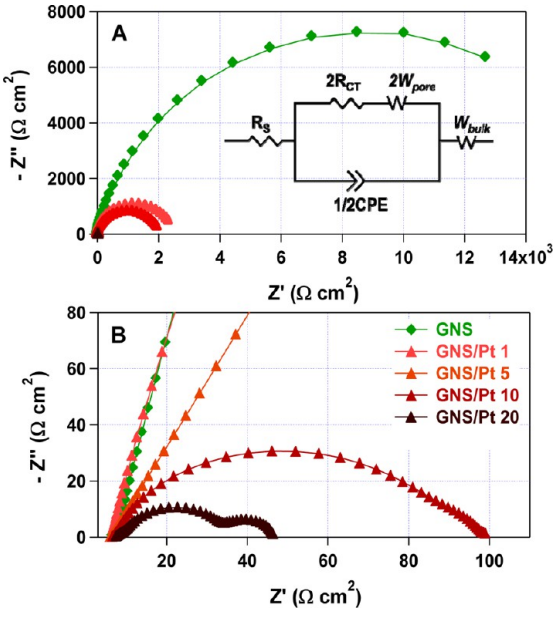

Figure 5. Nyquist plots of symmetrical cells. (A) Nyquist plot of entire frequency measured, and the equivalent circuit diagram (inserted figure: R_S is the series resistance, R_{CT} is the charge transfer resistance at the CE/electrolyte interface, W_{pore} is the Warburg impedance within CE layers, CPE is constant phase element of one electrode, and W_{bulk} is the Warburg impedance between the two CEs. (B) Amplified Nyquist plot for the higher-frequency region.

redox couples was filled in between. Generally, the high-frequency (left) semicircle indicates the electrochemical charge transfer resistance at the CE/electrolyte interface (R_{CT}), whereas the low-frequency (right) semicircle indicates Nernst diffusion-limited impedance of the I^-/I_3^- redox species in the electrolyte (R_D) (also, refer the graphs in Figure 5).[12,62] The plots were fitted with an equivalent circuit, shown in the inset of Figure 5A, consisting of the R_{CT} in parallel with a constant phase element (CPE), both of which are in series with the Warburg impedance within electrode pores (W_{pore}) and sheet resistance (R_{Sh}). The R_{CT} value of the symmetric cells of the GNS-CE/electrolyte interface was 1.7×10^4 Ω cm^2. As the loading of Pt-NPs increased in the NHB-CEs, the R_{CT} values decreased significantly. With only 5 wt % of loading the R_{CT} was reduced by one order (GNS/Pt5), and the R_{CT} of GNS/Pt20 was 27 Ω cm^2, which is $\sim 1 \times 10^3$ times lower than that of the GNS-CEs. The thickness of the GNS and NHB films was <100 nm, thus the capacitance effect of the mesoporous film was negligible.[12] The values by the EIS analysis of the symmetric cells are list in Table 1.

Table 1. EIS Analysis Result of Symmetric Cells Using GNS and GNS/Pt-NHB-Based CEs

CE	R_{Sh} (Ω cm^2)	R_{CT} (Ω cm^2)	(R_S[a] = R_{Sh} + R_{CT})/Ω cm^2
GNS	7.36	17251	17258
GNS/Pt1	6.17	2507	2513
GNS/Pt5	6.37	2220	2226
GNS/Pt10	6.82	86	92
GNS/Pt20	7.97	27	35

[a] R_S indicate the series resistance of the CEs, which is addition of R_{sh} and R_{CT}.

Cyclic voltammetry (CV) analysis is a powerful tool to investigate the electrocatalytic activity of CEs. The three types of CEs were placed in a CH_3CN solution containing 0.1 M $LiClO_4$, 5 mM LiI, and 0.5 mM I_2, and the samples were then used as working electrodes. The deposition area for all the CEs was ~0.4 cm^2 and the thickness of the GNS and GNS/Pt-NHB films was ~100 nm. It is known that the redox pair at the more negative potentials is due to reaction $I_3^- + 2e^- \rightarrow 3I^-$, while the redox pair at the more positive potentials is the redox pair of $3I_2 + 2e^- \rightarrow 2I_3^-$.[63,64] The left pair of peaks, which show the I^-/I_3^- redox process, is of interest for the performance of CEs. All three CEs showed the characteristic CV curves of the I^-/I_3^- redox pairs, whereas the CVs of bare FTO did not display any peak. The peak-to-peak separation (E_{pp}) of the left pairs can elucidate redox reaction kinetics at the CEs. The GNS-CEs showed much wider E_{pp} (0.64 V) compared to Pt-CEs (0.23 V), indicating their slower redox reaction rate. However, the value of E_{pp} was reduced considerably in NHB-CEs (0.30 V) and was nearly comparable to that of Pt-CEs. This fact indicated that loading of a small amount of Pt-NPs can significantly reduce the overpotential for the I_3^- reduction, resulting in the enhancement of the reaction kinetics. In our previous study, the more sluggish redox reaction kinetics of chemically prepared GNS-CEs than Pt-CEs was reported. In that study, although the GNS-CEs could achieve performance comparable to that of Pt-CEs after optimization of their chemical structures and electronic/electrocatalytic properties by thermal treatment at 400 °C, their E_{pp} for the I^-/I_3^- redox reaction was not changed, indicating that the overpotential of GNS-CEs was intrinsically higher than that of Pt-CEs.[60] This fact reveals that the reduction of E_{pp} of GNS/Pt-NHBs is attributed to the doping of Pt-NPs on the surface of GNSs, which work well as a support for the Pt-NPs. The E_{pp} was gradually reduced as the amount of Pt-NPs on the GNS increased, as shown in Figure S1 in the Supporting Information. The peak exchange current (I_P), which is closely related to the amount of redox reaction occurring on the CEs, was significantly increased in the NHB-CEs compared to the GNS-CEs. Considering that the film thickness of the two films was approximately the same (~100 nm), which means that the surface area of the two CEs is nearly identical, the enhanced redox reaction in the NHB-CEs is mainly attributed to the improved reaction rate by Pt-NP doping on the GNSs. As shown in Figure 6, the I_P of the NHB-CEs was comparable

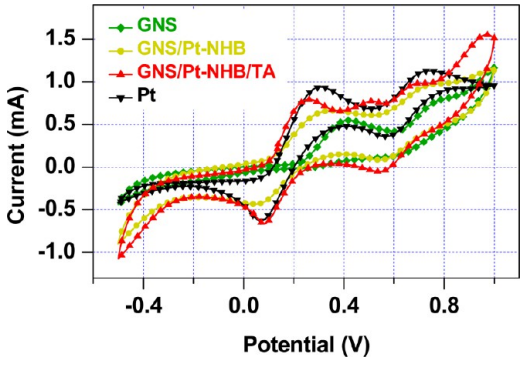

Figure 6. Cyclic voltammograms of GNS, GNS/Pt-NHBs (GNS/Pt20), and thermolytically prepared Pt-based CEs at a scan rate of 50 mV/s in a CH_3CN solution containing 0.1 M $LiClO_4$, 5 mM LiI, and 0.5 mM I_2. A Ag/Ag^+ reference electrode was used (10 mM $AgNO_3$ solution in the electrolyte).

(even slightly higher) than that of the Pt-CEs, even at a low thickness (~100 nm), indicating that our NHB-CEs have a sufficiently high electrocatalytic activity on the redox reaction.

Photovoltaic Performance of DSSCs. DSSCs were fabricated to demonstrate the performance of various CEs in a practical application. For DSSC fabrication, hierarchically structured submicrometer-sized TiO_2 spheres prepared by e-spraying commercial P25 nanoparticles were used as photoanodes (refer to our previous report for the detailed method).[65] The N719 (Solaronix) sensitizer was loaded on the surface of the photoelectrodes by immersing the electrodes in a dilute alcoholic solution, followed by incubating overnight. Finally, a conventional organic liquid electrolyte was injected into the pre-assembled cells, in which the graphene-based CEs were used to complete the sandwich-type cells (details of cell fabrication are in the Experimental Section). Figure 7 shows the

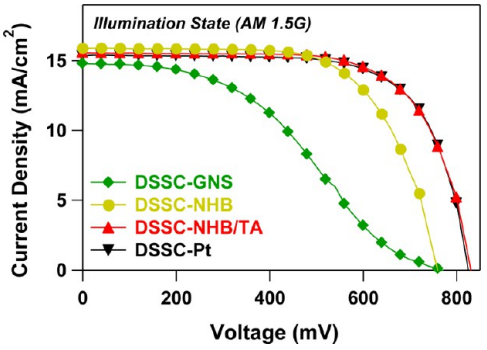

Figure 7. $J-V$ characteristics under 1 sun illumination (AM 1.5G, 100 mW cm^{-2}) of the DSSCs using GNS-, NHB- and thermolytically prepared Pt-CEs.

current density-voltage ($J-V$) characteristics of the DSSCs using various CEs under one sun illumination (AM 1.5G, 100 mW cm^{-2}). The reference Pt-CEs were prepared by the thermal reduction method, in which a Pt precursor ($H_2PtCl_6{\cdot}H_2O$) was drop-casted on the FTO/glass, followed by thermal treatment at 450 °C for 20 min. This method is known to form state-of-the-art CEs for DSSCs.[5,7] The PCE of the cells using GNS/Pt20 as a CE (DSSC-NHB) was approximately two times higher (PCE = 7.97%; V_{OC} = 760 mV, J_{SC} = 15.88 mA, FF = 66%) than that of the cells using GNS-CEs (DSSC-GNSs) (PCE = 4.44%; V_{OC} = 770 mV, J_{SC} = 14.78 mA cm^{-2}, FF = 39%), which indicates the reduction of overpotential for the I^-/I_3^- redox reaction by the Pt-NPs hybridization on GNSs was successfully reflected in the performance enhancement of DSSCs. The PCE of DSSC-NHB was ~90% compared to that of the reference cell DSSC-Pt that used a state-of-the-art CE (PCE = 8.85%; V_{OC} = 830 mV, J_{SC} = 15.23 mA cm^{-2}, FF = 70%). The values from the $J-V$ characteristic curves are listed in Table 2.

Table 2. $J-V$ Analysis Results of DSSCs Using Pt, GNS, and GNS-NHB (GNS-Pt20)-Based CEs

CE	V_{OC} (mV)	J_{SC} (mAcm^{-2})	FF (%)	PCE (%)
Pt	830	15.23	70	8.85
GNS	770	14.78	39	4.44
GNS-NHB	760	15.88	66	7.97
GNS-NHB-TA	830	15.56	69	8.91

Doping of Pt-NPs on GNSs could considerably improve the electrocatalytic activity of the CEs of DSSCs; however, the improvement was not as high as that of the state-of-the-art Pt-CEs that are prepared by thermal crystallization. To further optimize the performance of NHB-CEs, we subjected them to post-thermal annealing (TA) at 400 °C for 4 h under argon. The effect of TA on the chemical structure and physical properties of GNSs has been discussed in our earlier report.[60] In that report, the performance of thin-film CEs using chemically driven GNSs was significantly improved as a result of enhanced electrical conductivity. The removal of surface functional groups on GNSs by TA could restore the sp^2 conjugation on the basal plane, thus enhancing the charge transport within GNS films.[60] The TA of our NHB-CEs can lead one to expect an improvement of electrical properties of GNSs, as well as an improvement in the crystallinity of Pt, resulting in further optimization of CE performance. The cell efficiency of TA-treated DSSC-NHB (DSSC-NHB/TA) was further enhanced to 8.91% (V_{OC} = 830 mV, J_{SC} = 15.56 mA cm^{-2}, FF = 69%), which is comparable to that of DSSC-Pt (8.85%). As shown in the CV curves in Figure 6, the electrocatalytic activity of the NHB-CEs was further improved after TA, which is comparable to that of Pt-CEs. This facilitated consumption of I_3^- to I^- was reflected to the increased V_{OC} of DSSC-NHB/TA.[66]

CONCLUSIONS

Water-dispersible nanohybrids of GNSs and Pt were successfully prepared by the reduction of their precursors using vitamin C. The GNS/Pt-NHBs had a morphology in which uniformly sized Pt nanoparticles were well dispersed on the surface of the GNSs, and the amount of Pt could be precisely controlled. Sufficient colloidal stability of the NHBs enabled us to apply the e-spray method for the fabrication of thin film-based CEs for DSSCs (with film thicknesses of ~100 nm). The NHB-CEs displayed superior electrocatalytic activity and interfacial charge transfer for the redox process of I^-/I_3^- couples compared to the GNS-CEs. The addition of a small amount of Pt-NPs (<10 wt %) could significantly reduce the overpotential for the I_3^- reduction, resulting in boosting of the reaction kinetics identical to that of Pt-CEs. The enhanced reaction kinetics of NHB-CEs was well reflected in the performance of the DSSCs. The PCE of the DSSC-NHBs (7.97%) was approximately two times higher than that of the DSSC-GNSs (4.44%). When the NHB-CEs were optimized by TA, the performance of DSSC-NHB/TA (PCE = 8.91%) was comparable to or slightly better than that of DSSC-Pt (PCE = 8.85%), in which a state-of-the-art Pt-CE was used. Our GNS/Pt-NHBs can be easily prepared by simple one-pot green chemistry in aqueous media, and their e-sprayed thin films form very efficient CEs for DSSCs, indicating that the GNSs effectively work as a support for the Pt-NPs.

EXPERIMENTAL SECTION

Preparation of GNS/Pt-NHBs. Graphene oxides (GO) was synthesized by the modified Hummer's method[50,51] using graphite powder. In order to make a stable aqueous suspension, ultra-sonication was performed on the GO/H_2O solution (25 mg of GO in 250 mL of H_2O). An aqueous Pt precursor (H_2PtCl_6) solution (1 wt %) was added drop-wise into the aqueous GO solution to reach various Pt precursor/GO ratios. Ultrasonication was performed again for 30 min to disperse the Pt precursor throughout the GO sheets. As a reduction agent, 500 mg of vitamin C (ascorbic acid) was added to the solution.

The as-prepared solution was kept at 25 °C for 48 h under vigorous stirring. After that, centrifugation was conducted several times to remove any remaining ascorbic acid and unattached Pt particles from the solution. Subsequently, microfiltration and sonication was performed for 3 cycles. The concentration of the final solution was 0.3 mg mL^{-1} in water.

Preparation of GNS/Pt-NHB-Based CEs. The fluorine-doped tin oxide (FTO) glass (TEC-8, Pilkington) was drilled using a diamond-tipped microdrill, washed with 0.1 M HCl solution in ethanol, and subsequently cleaned in an ultrasonic bath with H_2O/EtOH for 15 min. In order to prepare NHB-CEs, a 0.16 mg mL^{-1} NHB solution in a DI-water/ethanol (6/4) solution was electrosprayed. First, the aqueous NHB solution was loaded into a plastic syringe that had a metallic microtip connected to a high-voltage power supply (BERTAN SERIES 205B). An electric field of 1.6 $kVcm^{-1}$ was applied between the metallic microtip and the conducting FTO glass at a feed rate of 30 $\mu L\ min^{-1}$. To form a uniform NHB film for CEs in a wide area, an x-y motion control system was adopted during the electrospray process. For thermal treatment, the NHB-CEs were heated at 400 °C for 4 h under argon atmosphere. GNS-CEs were fabricated using an identical procedure using a 0.16 mg mL^{-1} aqueous GNS solution.

Device Fabrication. For the preparation of TiO_2 sphere-based photoelectrodes, 10 wt % P25 (Degussa) nc-TiO_2 was dispersed in ethanol using an ultra-apex mill (Model UAM-015, Kotobuki). The dispersed solution was electrosprayed onto a washed FTO glass samples in the same manner as with the CE preparation. After electrospraying, the as-prepared TiO_2 spheres were placed between two steel plates and laminated under a pressure of 12 MPa. The pressed TiO_2 sphere-coated FTO glass samples were sintered under air conditions at 500 °C for 30 min to complete the fabrication of the photoelectrodes layers. After cooling to 80 °C, a TiO_2 photoelectrode was immersed into the purified 3×10^{-4} M *cis*-di (thiocyanato)-N,N′-bis (2,2′-bipyridyl-4-carboxylic acid-4′-tetrabutylammonium carboxylate) ruthenium(II) (N719, Solaronix) solution for 15 h at room temperature. A dye-adsorbed TiO_2 photoelectrode was assembled and sealed with the CEs using thermal adhesive films (Surlyn, Dupont 1702, 25-μm-thick) to provide a space between the electrodes. The Pt-CE was prepared by drop-casting 5 mM H_2PtCl_6 in isopropyl alcohol onto the drilled FTO glass and then sintering the glass at 400 °C for 20 min under air condition. A liquid electrolyte consisting of 0.65 M 1-butyl-3-methylimidazolium iodide (BMII), 0.5 M 4-*tert*-butylpyridine (TBP), 0.03 M iodine (I_2), and 0.05 M guanidiniumthiocyanate (GSCN) in a mixture of acetonitrile and valeronitrile (85:15, v/v) was introduced through a drilled hole on the CE side. The holes were subsequently sealed with a cover glass.

Material Characterization. The morphology of e-sprayed GNS/Pt-NHB thin films on FTO was characterized using field-emission scanning electron microscopy (FE-SEM, Hitachi S-4100), transmission electron microscopy (TEM, Philips CM30), and high-resolution transmission electron microscopy (HR-TEM, Tecnai G^2). X-ray diffraction (XRD) patterns were investigated at room temperature using an X-ray diffractometry system (Bruker, D8 DISCOVER). Loaded amounts of Pt nanoparticles on GNS/Pt-NHBs were measured using inductively coupled plasma atomic emission spectrometer (ICP-AES, Thermo PolyScan-61E). IR and UV-vis spectra were recorded on a Fourier transform infrared spectroscope (FT-IR, Thermo Scientific, NICOLET iS10) and a UV-vis spectrophotometer (UV-Vis, JASCO, V-670), respectively. Chemical properties of GNS/Pt-NHBs were investigated using X-ray photoelectron spectroscopy (XPS, ULVAC-PHI, PHI-5000) and Raman spectroscopy (Raman, LabRAM HR, Horiba) The film thickness of the GNS/Pt-NHB CEs was measured using a surface profiler (P-10, Tencor). Specific surface area (Brunauer–Emmett–Teller, BET) and pore volumes (Barrett–Joyner–Halenda, BJH) were investigated using Sorptomatic® (Micromeritics Instrument, TriStar II 3020)

Electrochemical Measurements. The current density-voltage measurements were recorded on a Keithley 2400 source measuring system. A class A solar simulator (Newport, model 91195A-1000) with a 450 W Xe lamp was used as a light source, and a NREL-calibrated mono-Si solar cell provided a BF-7 filtered light intensity to approximately AM 1.5G, 1 sun. The electrochemical impedance spectra (EIS) measurements were performed using a potentiostat (Solartron 1287)-connected frequency response analyzer (Solartron, SI 1260) at an amplitude of 10 mV and an open circuit voltage (V_{OC}) under 100 mW cm^{-2} of illumination. Cyclic voltametric measurements were recorded on a potentiostat (Bio-Logic SA, VSP-CHAS) in a three-electrode system with the various CEs as the working electrode, a Pt foil counter electrode, and a Ag/Ag^+ reference electrode (0.01 M $AgNO_3$ in acetonitrile) soaked in an acetonitrile solution containing 0.1 M $LiClO_4$, 5 mM LiI, and 0.5 mM I_2 at a scan rate of 50 mVs^{-1}.

■ ASSOCIATED CONTENT

Ⓢ Supporting Information

Cyclic voltammograms of GNS/Pt-NHBs (GNS/Pt1, GNS/Pt5, GNS/Pt10, GNS/Pt20). This material is available free of charge via the Internet at http://pubs.acs.org/.

■ AUTHOR INFORMATION

Corresponding Author

*E-mail: syjang@kookmin.ac.kr. Tel: +82-2-910-5768. Fax: +82-2-910-4415.

Notes

The authors declare no competing financial interest.

■ ACKNOWLEDGMENTS

The authors gratefully acknowledge the support from the Basic Science Research Program through the National Research Foundation of Korea (NRF, 2012045675 and 20110008698), funded by the Ministry of Education, Science, and Technology, and the Korea Research Council of Fundamental Science & Technology (KRCF) and KIST for "National Agenda Project (NAP)" program.

■ REFERENCES

(1) Hagfeldt, A.; Boschloo, G.; Sun, L.; Kloo, L.; Pettersson, H. *Chem. Rev.* **2010**, *110*, 6595–6663.
(2) O'Regan, B.; Grätzel, M. *Nature* **1991**, *353*, 737–740.
(3) Ito, S.; Chen, P.; Comte, P.; Nazeeruddin, M. K.; Liska, P.; Pechy, P.; Grätzel, M. *Prog. Photovolt: Res. Appl.* **2007**, *15*, 603–612.
(4) Papageorgiou, N.; Maier, W. F.; Grätzel, M. *J. Electrochem. Soc.* **1997**, *144*, 876–884.
(5) Hauch, A.; Georg, A. *Electrochim. Acta* **2001**, *46*, 3457–3466.
(6) Lee, Y.-L.; Chen, C.-L.; Chong, L.-W.; Chen, C.-H.; Liu, Y.-F.; Chi, C.-F. *Electrochem. Commun.* **2010**, *12*, 1662–1665.
(7) Murakami, T. N.; Grätzel, M. *Inorg. Chim. Acta* **2008**, *361*, 572–580.
(8) Chen, J. K.; Li, K. X.; Luo, Y. H.; Guo, X. Z.; Li, D. M.; Deng, M. H.; Huang, S. Q.; Meng, Q. B. *Carbon* **2009**, *47*, 2704–2708.
(9) Huang, Z.; Liu, X. H.; Li, K. X.; Li, D. M.; Luo, Y. H.; Li, H.; Song, W. B.; Chen, L. Q.; Meng, Q. B. *Electrochem. Commun.* **2007**, *9*, 596–598.
(10) Lee, W. J.; Ramasamy, E.; Lee, D. Y.; Song, J. S. *ACS Appl. Mater. Interfaces* **2009**, *1*, 1145–1149.
(11) Han, J.; Kim, H.; Kim, D. Y.; Jo, S. M.; Jang, S. Y. *ACS Nano* **2010**, *4*, 3503–3509.
(12) Kavan, L.; Yum, J. H.; Grätzel, M. *ACS Nano* **2011**, *5*, 165–172.
(13) Roy-Mayhew, J. D.; Bozym, D. J.; Punckt, C.; Aksay, I. A. *ACS Nano* **2010**, *4*, 6203–6211.
(14) Hasin, P.; Alpuche-Aviles, M. A.; Wu, Y. Y. *J. Phys. Chem. C* **2010**, *114*, 15857–15861.
(15) Kavan, L.; Yum, J. H.; Grätzel, M. *ACS Appl. Mater. Interfaces* **2012**, *4*, 6999–7006.
(16) Xia, J. B.; Masaki, N.; Jiang, K. J.; Yanagida, S. *J. Mater. Chem.* **2007**, *17*, 2845–2850.
(17) Lee, K. S.; Lee, H. K.; Wang, D. H.; Park, N.-G.; Lee, J. Y.; Park, O. O.; Park, J. H. *Chem. Commun.* **2010**, *46*, 4505–4507.

(18) Ahmad, S.; Yum, J. H.; Butt, H. J.; Nazeeruddin, M. K.; Grätzel, M. *ChemPhysChem* **2010**, *11*, 2814−2819.
(19) Ameen, S.; Akhtar, M. S.; Kim, Y. S.; Yang, O. B.; Shin, H.-S. *J. Phys. Chem. C* **2010**, *114*, 4760−4764.
(20) Li, Q. H.; Wu, J. H.; Tang, Q. W.; Lan, Z.; Li, P. J.; Lin, J. M.; Fan, L. Q. *Electrochem. Commun.* **2008**, *10*, 1299−1302.
(21) Wu, J.; Li, Q.; Fan, L.; Lan, Z.; Li, P.; Lin, J.; Hao, S. *J. Power Sources* **2008**, *181*, 172−176.
(22) Lee, K. S.; Lee, Y.; Lee, J. Y.; Ahn, J.-H.; Park, J. H. *ChemSusChem* **2012**, *5*, 379−382.
(23) Sun, H.; Luo, Y.; Zhang, Y.; Li, D.; Yu, Z.; Li, K.; Meng, Q. *J. Phys. Chem. C* **2010**, *114*, 11673−11679.
(24) Hong, W.; Xu, Y.; Lu, G.; Li, C.; Shi, G. *Electrochem. Commun.* **2008**, *10*, 1555−1558.
(25) Lin, C.-Y.; Lin, J.-Y.; Wan, C.-C.; Wei, T.-C. *Electrochim. Acta* **2011**, *56*, 1941−1946.
(26) Liu, C.-Y.; Huang, K.-C.; Wang, C.-C.; Ho, K.-C. *Electrochim. Acta* **2012**, *59*, 128−134.
(27) Kim, S. S.; Park, K. W.; Yum, J. H.; Sung, Y. E. *J. Photochem. Photobiol., A* **2007**, *189*, 301−306.
(28) Huang, K. C.; Wang, Y. C.; Dong, R. X.; Tsai, W. C.; Tsai, K. W.; Wang, C. C.; Chen, Y. H.; Vittal, R.; Lin, J. J.; Ho, K. C. *J. Mater. Chem.* **2010**, *20*, 4067−4073.
(29) Wang, H. Y.; Wang, F. M.; Wang, Y. Y.; Wan, C. C.; Hwang, B. J.; Santhanam, R.; Rick, J. *J. Phys. Chem. C* **2011**, *115*, 8439−8446.
(30) Peng, S.; Liang, J.; Mhaisalkar, S. G.; Ramakrishna, S. *J. Mater. Chem.* **2012**, *22*, 5308−5311.
(31) Gong, F.; Wang, H.; Wang, Z. S. *Phys. Chem. Chem. Phys.* **2011**, *13*, 17676−17682.
(32) Yen, M. Y.; Teng, C. C.; Hsiao, M. C.; Liu, P. I.; Chuang, W. P.; Ma, C. C. M.; Hsieh, C. K.; Tsai, M. C.; Tsai, C. H. *J. Mater. Chem.* **2011**, *21*, 12880−12888.
(33) Bajpai, R.; Roy, S.; Kumar, P.; Bajpai, P.; Kulshrestha, N.; Rafiee, J.; Koratkar, N.; Misra, D. S. *ACS Appl. Mater. Interfaces* **2011**, *3*, 3884−3889.
(34) Ruoff, R. *Nat. Nanotechnol.* **2008**, *3*, 10−11.
(35) Allen, M. J.; Tung, V. C.; Kaner, R. B. *Chem. Rev.* **2009**, *110*, 132−145.
(36) Wang, X.; Zhi, L. J.; Müllen, K. *Nano Lett.* **2008**, *8*, 323−327.
(37) Wu, J.; Agrawal, M.; Becerril, H. c. A.; Bao, Z.; Liu, Z.; Chen, Y.; Peumans, P. *ACS Nano* **2009**, *4*, 43−48.
(38) Avouris, P.; Chen, Z.; Perebeinos, V. *Nat. Nanotechnol.* **2007**, *2*, 605−615.
(39) Lu, C. H.; Yang, H. H.; Zhu, C. L.; Chen, X.; Chen, G. N. *Angew. Chem., Int. Ed.* **2009**, *48*, 4785−4787.
(40) Fowler, J. D.; Allen, M. J.; Tung, V. C.; Yang, Y.; Kaner, R. B.; Weiller, B. H. *ACS Nano* **2009**, *3*, 301−306.
(41) Qu, L. T.; Liu, Y.; Baek, J. B.; Dai, L. M. *ACS Nano* **2010**, *4*, 1321−1326.
(42) Stoller, M. D.; Park, S. J.; Zhu, Y. W.; An, J. H.; Ruoff, R. S. *Nano Lett.* **2008**, *8*, 3498−3502.
(43) Wang, C. Y.; Li, D.; Too, C. O.; Wallace, G. G. *Chem. Mater.* **2009**, *21*, 2604−2606.
(44) Kundu, P.; Nethravathi, C.; Deshpande, P. A.; Rajamathi, M.; Madras, G.; Ravishankar, N. *Chem. Mater.* **2011**, *23*, 2772−2780.
(45) Qiu, J. D.; Wang, G. C.; Liang, R. P.; Xia, X. H.; Yu, H. W. *J. Phys. Chem. C* **2011**, *115*, 15639−15645.
(46) Yoo, E.; Okata, T.; Akita, T.; Kohyama, M.; Nakamura, J.; Honma, I. *Nano Lett.* **2009**, *9*, 2255−2259.
(47) Guo, S.; Wen, D.; Zhai, Y.; Dong, S.; Wang, E. *ACS Nano* **2010**, *4*, 3959−3968.
(48) Dey, R. S.; Raj, C. R. *J. Phys. Chem. C* **2010**, *114*, 21427−21433.
(49) Qin, W.; Li, X. *J. Phys. Chem. C* **2010**, *114*, 19009−19015.
(50) Kou, R.; Shao, Y. Y.; Wang, D. H.; Engelhard, M. H.; Kwak, J. H.; Wang, J.; Viswanathan, V. V.; Wang, C. M.; Lin, Y. H.; Wang, Y.; Aksay, I. A.; Liu, J. *Electrochem. Commun.* **2009**, *11*, 954−957.
(51) Hummers, W. S.; Offeman, R. E. *J. Am. Chem. Soc.* **1958**, *80*, 1339−1339.
(52) Stankovich, S.; Dikin, D. A.; Piner, R. D.; Kohlhaas, K. A.; Kleinhammes, A.; Jia, Y.; Wu, Y.; Nguyen, S. T.; Ruoff, R. S. *Carbon* **2007**, *45*, 1558−1565.
(53) Si, Y. C.; Samulski, E. T. *Chem. Mater.* **2008**, *20*, 6792−6797.
(54) Kim, S. J.; Park, Y. J.; Ra, E. J.; Kim, K. K.; An, K. H.; Lee, Y. H.; Choi, J. Y.; Park, C. H.; Doo, S. K.; Park, M. H.; Yang, C. W. *Appl. Phys. Lett.* **2007**, *90*, 023114−3.
(55) Li, D.; Muller, M. B.; Gilje, S.; Kaner, R. B.; Wallace, G. G. *Nat. Nanotechnol.* **2008**, *3*, 101−105.
(56) Stankovich, S.; Piner, R. D.; Chen, X. Q.; Wu, N. Q.; Nguyen, S. T.; Ruoff, R. S. *J. Mater. Chem.* **2006**, *16*, 155−158.
(57) Fernandez-Merino, M. J.; Guardia, L.; Paredes, J. I.; Villar-Rodil, S.; Solis-Fernandez, P.; Martinez-Alonso, A.; Tascon, J. M. D. *J. Phys. Chem. C* **2010**, *114*, 6426−6432.
(58) Zhang, J. L.; Yang, H. J.; Shen, G. X.; Cheng, P.; Zhang, J. Y.; Guo, S. W. *Chem. Commun.* **2010**, *46*, 1112−1114.
(59) Gao, J.; Liu, F.; Liu, Y. L.; Ma, N.; Wang, Z. Q.; Zhang, X. *Chem. Mater.* **2010**, *22*, 2213−2218.
(60) Jang, S.-Y.; Kim, Y.-G.; Kim, D. Y.; Kim, H.-G.; Jo, S. M. *ACS Appl. Mater. Interfaces* **2012**, *4*, 3500−3507.
(61) Rietveld, I. B.; Suganuma, N.; Kobayashi, K.; Yamada, H.; Matsushige, K. *Macromol. Mater. Eng.* **2008**, *293*, 387−399.
(62) Trancik, J. E.; Barton, S. C.; Hone, J. *Nano Lett.* **2008**, *8*, 982−987.
(63) Boschloo, G.; Hagfeldt, A. *Acc. Chem. Res.* **2009**, *42*, 1819−1826.
(64) Popov, A. I.; Geske, D. H. *J. Am. Chem. Soc.* **1958**, *80*, 1340−1352.
(65) Hwang, D.; Lee, H.; Jang, S. Y.; Jo, S. M.; Kim, D.; Seo, Y.; Kim, D. Y. *ACS Appl. Mater. Interfaces* **2011**, *3*, 2719−2725.
(66) Huang, S. Y.; Schlichthörl, G.; Nozik, A. J.; Gratzel, M.; Frank, A. J. *J. Phys. Chem. B* **1997**, *101*, 2576−2582.